Assessment of ferroptosis inducers and Nrf2 inhibitors as radiosensitisers in 2D and 3D breast cancer cell cultures

Alzufairi AA, Souilhol C, Jordan-Mahy N, *Cross NA.

Biomolecular Sciences Research Centre, Sheffield Hallam University, Howard Street, Sheffield, S1 1WB, UK.

Email: n.cross@shu.ac.uk

*Corresponding author

Key words:

Ferroptosis, Nrf2, irradiation, radiotherapy, radiosensitiser, 3D cell culture, RSL3, Erastin, FIN56, ML385

Abstract

Ferroptosis is a form of programmed cell death that is modulated in some cancer cells as a pro-survival mechanism. Induction of ferroptosis is a potential anti-cancer strategy, and enhancement of ferroptosis using ferroptosis inducers has the potential to enhance current anti-tumour mechanisms. In this study, we assessed the effect of the ferroptosis inducers Erastin, RSL-3 and FIN-56 on radiosensitivity in 2D cell culture, and in 3D alginate tumour spheroids from breast cancer cell lines. Since some tumours modulate ferroptosis via increased Nrf2 production, and MCF-7 and MDA-MB-231 both produce Nrf2 protein, we also assessed the effects of the Nrf2 inhibitor ML385 on radiosensitivity. MDA-MB-231 was highly sensitive to all ferroptosis inducers, and ferroptosis was reversed by the ferroptosis inhibitors Ferrostatin-1, Liproxstatin-1 and Deferoxamine. MCF-7 was resistant to all ferroptosis inducers. MDA-MB-231 and MCF-7 cells were sensitive to irradiation in 2D cell culture but resistant to irradiation in 3D alginate spheroids. Ferroptosis inducers did not synergistically enhance irradiation-induced cell death in 2D cell cultures. There was also no robust enhancement to irradiation effects with ferroptosis inducers in 2D or 3D cell culture. Ferroptosis inducers did, however, show a heterogeneous response in 3D cell culture, in that isogenic spheroids responded differently within the same spheroid. The Nrf2 inhibitor ML385 showed no synergistic enhancement of ferroptotic cell death when combined with irradiation. These studies suggest targeting ferroptosis does not induce short-term enhancement of ferroptotic cell death.

Introduction

Ferroptosis is a recently discovered form of cell death established in 2012 by the work of Dixon and his colleagues (Dixon *et al.*, 2012). This form of death is an iron-dependent programme of cell death that is induced by lipid peroxidation. It is characterised by the accumulation of reactive oxygen species (ROS) which induces lipid peroxidation (Dixon *et al.*, 2012), causing morphological features differently from other forms of programmed cell death. Inducers of ferroptosis typically target either glutathione peroxidase 4 (GPX4), which protect against lipid peroxidation and is reliant on glutathione, or target glutathione biosynthesis (Sui *et al*, 2018). For example, Erastin directly inhibits system Xc-, which is the cystine/glutamate antiporter crucial for subsequent glutathione biosynthesis from cysteine and glutamate (Dixon *et al*, 2014). Likewise, Ras Synthetic Lethal-3 (RSL3) binds and inactivates GPX4, leading to accumulation of lipid peroxidation, which leads to ferroptotic cell death (Tang *et al,* 2021). FIN56 induces GPX4 degradation although the mechanism is unclear (Shimada *et al*, 2016). Ferroptosis can be inhibited using a panel of small molecule ferroptosis inhibitors. Deferoxamine is an iron chelator, and since ferroptosis is reliant on intracellular iron, via Fenton-type chemistry to induce lipid peroxidation, iron chelation potently inhibits ferroptosis. Deferoxamine is a classic iron-chelating ferroptosis inhibitor that can be used to prevent ferroptosis and damage to normal cells and tissues (Wu *et al*, 2020, Kose *et al*, 2019). Liproxstatin-1 and Ferrostatin-1 are potent inhibitors of lipid peroxidation and are able to reverse ferroptosis in $GPX4^{-/-}$ cells and in response to ferroptosis inducers (Zilka *et al*, 2017). However, Liproxstatin-1, could not rescue cells dying by apoptosis or necroptosis, indicating that it is a specific inhibitor of ferroptosis (Feng et al, 2019). Liproxstatin-1 also has been shown to significantly increase the protein levels of nuclear factor erythroid 2-related factor 2 (Nrf2), the master regulator of the antioxidant response, which helps to promote cell survival (Feng *et al,* 2019). Both Erastin and RSL3 inhibit the ferroptosis pathway in cancer cells by disturbing the redox homeostasis and allowing the iron-independent accumulation of lethal ROS (Dixon *et al*, 2012). Dolma *et al.,* (2003) identified two structurally unrelated small molecules, named Erastin and RSL3, that were selectively lethal to oncogenic Ras mutant cell lines, and which are referred to together as RAS-selective lethal (RSL) compounds (Dolma et al, 2003). Ferroptosis can be induced by blocking system Xc- with small molecule ferroptosis inhibitors such as Erastin. Ferroptosis can also be induced by inhibition of GPX4 stability or activity using FIN56 or RSL3 respectively (Dixon *et al*, 2014). Erastin can reduce cellular GSH levels by inhibiting system Xc- directly, reducing cystine and glutamate uptake which are crucial for glutathione production. Loss of glutathione renders cells very susceptible to lipid peroxidation. RSL3 induces ferroptosis by targeting GPX4 directly (Yang and Stockwell, 2008).

Irradiation is known to induce cell death by generating ROS, depleting glutathione, and activating targets such as acyl-CoA synthetase long-chain family member 4 (ACSL4). ACSL4 alters cellular lipid composition and in effect, is an essential component of the ferroptosis-inducing pathway (Doll *et al,* 2017). Furthermore, ferroptosis is a key mediator of radiation-induced injury (Su *et al*, 2022), and ferroptosis inhibition mitigates radiation-induced injury. Recent studies have identified GPX4 inhibitors that potentiate irradiation responses in a ferroptosis-dependent manner (Lui *et al,* 2023). Furthermore, ferroptosis inhibitors can reverse radiation-induced cell death, whereas the ferroptosis inducer RSL3 enhances it (Ye *et al,* 2021). Therefore, we hypothesised that ferroptosis inducers would enhanced radiotherapy responses in breast cancer cells, and we have expanded these studies to 3D cell culture models. Furthermore, Nrf2 is a master regulator of the antioxidant response and is intrinsically linked in to modulating ferroptosis signalling (He *et al.* 2020). It is sequestered by Kelch-like ECH-associated protein 1 (Keap-1), and in the presence of reactive oxygen species, it is released (Baird and Yamamoto, 2020). Furthermore, Nrf2 is a prerequisite for 3D spheroid formation, and the knockdown of Nrf2, prevents spheroid formation; presumably due to the loss of an antioxidant response (Takahashi *et al,* 2020). The specific role of Nrf2 in mediating radio-responses in 3D cell culture is not known. Nrf2 is known to respond to irradiation and DNA damage, which is mediated by an increase in glutathione during irradiation exposure (Schäfer *et al,* 2010). Furthermore, radio-resistance in breast cancer stem cells have been linked to the activation of the Keap1-Nrf2 axis (Kamble *et al,* 2021). Additionally, Nrf2-inibition using ML385, sensitised breast cancer stem cells to ionising radiation, showing that irradiation-induced ROS can activate Nrf2, counteracting the irradiation-induced damage (Qin *et al,* 2021). Therefore Nrf2 inhibition might be a potent radio-sensitising strategy (Qin *et al,* 2021). Although studies have focussed on cancer stem cells in breast cancer, studies have not directly assessed the cellular responses to irradiation in tumour spheroids. It is therefore hypothesised that ferroptosis inducers increase death after irradiation of both 2D and 3D breast cancer cell culture models, and that this is reversed by ferroptosis inhibitors.

Materials and methods

Cell culture

MCF-7 and MDA-MB-231 (ECACC) were cultured in Dulbecco's Modified Eagle Medium (DMEM) (Lonza, Manchester, UK), supplemented with 10% (v/v) heat-inactivated foetal bovine serum (FBS) (Lonza) and 1% of 100 IU penicillin and 100 µg/ml streptomycin (ThermoFisher Scientific, Altrincham, UK). Both cell lines were cultured in T75 flasks (ThermoFisher Scientific) incubated at 37°C under 5% CO_2. Cell viability of trypan blue stained cells was determined prior to all studies and percentage of viability was measured using the Countess™ automated cell counter (ThermoFisher Scientific). For cell treatments in 2D cell culture, cells were plated at $1x10^4$ cells/well in a 96-well plate and left to adhere for 24 hours prior to treatment.

Treatment of cells with ferroptosis inducers and inhibitors

Cells were treated with either RSL3 (Sigma, Poole, UK), Erastin (Selleck Chem, Ely, UK) or FIN56 (Sigma) at 0, 1.25, 2.5, 5 or 10 µM in the presence or absence of the ferroptosis inhibitors Deferoxamine (Selleck Chemical company Ely, UK) at 10 µM, Liproxstatin-1 (Sigma) at 1 µM or Ferrostatin-1 (Sigma) at 1 µM. For ML385 treatments, cells were treated with 10 µM ML385 (Sigma). All treatments and controls contained a final concentration of 0.2% Dimethyl sulfoxide (DMSO) as a vehicle control. All treatments were carried out in triplicate in three technical repeats.

Irradiation of cells

Cells were either plated in 96 well plates at a cell density of $1x10^5$ cells/ml or for colony formation assays, prepared at $1x10^5$ cells/ml of medium in a falcon tube and transported to University of Sheffield for irradiation. Cells were exposed to a ^{137}Cs source delivering 1Gy per 28 seconds at 0.6MeV. After irradiation, cells were transported to Sheffield Hallam University and either treated with ferroptosis inducers and/or ML385 or plated out for colony formation assays. In all experiment, a control plate or tube of cells was mock-irradiated, including travel to University of Sheffield to account for time outside of the incubator.

Assessment of cell death using Hoechst 33342 and propidium iodide staining

Hoechst 33342 and propidium iodide (PI) staining was used to assess cell death. After cell treatments, cells were stained with Hoechst 33342 (Sigma) and PI (Sigma) at a final concentration 10 µg/ml Hoechst 33342 and 10 µg/ml PI and incubated for 30 minutes at 37°C. Cells were examined using an IX81 or IX70 fluorescence microscope (Olympus) and images captured using

Cell-F software (Olympus). Cells were counted manually, and the percentage of apoptosis was calculated based on duplicate representative fields of view each containing at least 100 cells.

CellTiter-Glo® luminescent cell viability assay

The CellTiter-Glo® luminescent cell viability assay measures the level of ATP precent in living cells, an indicator of metabolic activity within the cells. For ATP measurement, cells were seeded in white 96-well plates (Fisher Scientific) at 1 x 10^4 cell per well and treated with each ferroptosis inducers (RSL3, Erastin, FIN56) alongside a 0.2% (v/v) DMSO vehicle control for 24 hours. After treatments, 25 µl of CellTiter-Glo® reagent from CellTiter-Glo® luminescent cell viability assay kit (Promega, Southampton, UK) was added to each well and mixed for 2 minutes on a plate shaker and incubated at room temperature (RT) for 10 minutes to stabilize the luminescent signal. The luminescent signal was measured by a luminometer detector using CLARIOstar plate reader (BMG Labtech, Ortenberg, Germany). The luminescence is proportional to the total ATP present within each well. The average from three luminescence measurements was calculated and all treated cells were normalized to the vehicle controls, which was assigned a 100% ATP activity. All treatments were performed in triplicate, in three independent experiments.

3D Alginate cell culture assay

MDA-MB-231 and MCF-7 cultured cells were trypsinized, washed with PBS (Lonza), and resuspend in 0.15M NaCl and counted. Cells were centrifuged at 400g for 5 mins and the cell pellet containing 1x10^6 cells was resuspended in 1mL of a sterile 1.2% (w/v in Saline) sodium alginate (Sigma) and dropped into 15-20 ml of sterile 0.2M $CaCl_2$ in a 50ml falcon tube using a 21G needle (Sigma-Aldrich). This solution was then incubated at 37^{o}C for 5 minutes. Beads were then washed twice in 15ml sterile 0.15M NaCl, for 5 minutes. Finally, 20ml of medium was added to the alginate beads and cultured in an upright T25 flask at 37°C under 5% CO_2, for up to 14 days prior to treatment.

CellTiter-Glo® 3D cell viability assay

For ATP measurement, alginate spheres were seeded in white 96-well plates (Fisher Scientific) with one alginate bead per well and treated with each ferroptosis inducer (RSL3, Erastin, FIN56), alongside a 0.2% (v/v) DMSO vehicle control. Treated cells were incubated at 37°C with 5% CO_2, for 48 hours. After treatments, 100 µl of CellTiter-Glo® reagent from CellTiter-Glo® 3D cell viability assay kit (Promega-UK) was added to each well and mixed for 5 minutes on a plate shaker and incubated at room temperature (RT) for 25 minutes to stabilize the luminescent signal. The luminescent signal was measured by a luminometer detector using a CLARIOstar plate reader.

The average from at least 4 luminescence measurements was calculated and all treated cells were normalized to the controls.

Immunocytochemistry to detect Nrf2

Untreated MCF-7 and MDA-MB-231 cells were seeded at 2 x 10^4 cell per well on 8-well glass chamber slides (™ Nunc™ Lab-Tek™ II Chamber Slide™, Thermo Scientific). Cells were left to adhere for 24 hours in a 5% CO_2 incubator at 37°C. Cells were fixed in 50:50 acetone/methanol in a Coplin jar in the fume hood for 10-15 min, washed in Tris-buffered saline (TBS) for 5 minutes, followed by blocking for 15 minutes with goat serum (25 % in TBS), then washed with TBS for 5 minutes. Cells were incubated with a 1:200 dilution of primary Nrf2 antibody (Nrf2 (D1Z9C) XP® rabbit mAb (Cell Signalling Technology, Danvers, USA) for 2 hours. After incubation, cells were washed three times in TBS and dried, incubated with secondary antibody (anti-rabbit IgG (H+L), F(ab')2 Fragment (Alexa Fluor® 488 conjugate) (Cell Signalling Technology) in a 1:500 dilution in TBS for 2 hours at room temperature in the dark. After incubation cells were washed three times with TBS, then the nuclei were stained with a mounted 4,6-diamidino-2-phenyindole (DAPI) (Sigma) and imaged using a Zeiss LMS 800 confocal microscope.

Results

The effects of ferroptosis inducers and inhibitors on breast cancer cells

The effects of ferroptosis inducers on cell death of MB-MDA-231 cells and MCF-7 cells was detected using fluorescent microscopy images after staining with Hoechst 33342 and PI. Live cells and apoptotic cells are stained blue with Hoechst 33342, dead cells are stained red with PI staining. The percentage of cell death was counted after 24 hours treatment for three independent experiments. Any cell with evidence of PI positivity was classed as dead, as these cells have permeabilised membranes. Due to co-staining with Hoechst 33342, dead cells appear pink, or red, on images (Figure 1A).

The ferroptosis inducer RSL3 induced significant cell death at all doses tested from 0.075 μM in MDA-MB-231 cells with greater than 50% cell death at 0.075 μM (Figure 1B). For subsequent combination studies, the optimum dose for combination studies was determined to be 0.0375 μM. MDA-MB-231 cells were highly sensitive to Erastin, showing significant cells death at all doses above 0.15 μM (Figure 1C). Therefore 0.15 μM was considered a suitable dose for combination studies, whereas 10 μM was shown to be a suitable positive control dose for studies with ferroptosis inhibitors to establish that cell death was indeed ferroptotic. Propidium iodide-positive cells did not appear to be apoptotic in morphology with absence of pycnotic and condensed nuclei, although this was not formally quantified. The ferroptosis inducer FIN56 induced significant cell death at all doses tested from 0.15 μM, (Figure 1D). Since this dose induced a small, but significant amount of cell death (15%), this was appropriate for use in combination studies with radiotherapy. As with RSL3 and Erastin, dead cells did not appear to be apoptotic in morphology.

The effect of ferroptosis inducers is reversed by ferroptosis inhibitors in MDA-MB-231 cells

RSL3 (10 μM) significantly and potently induced cell death in MDA-MB-231 cells (Figure 1E). To establish whether this cell death was likely to be ferroptosis, co-incubation with three ferroptosis inhibitors with differing mechanisms of action was tested. The cell death induced by RSL3 was completely or partially reversed by ferroptosis inhibitor Deferoxamine, Liproxstatin-1, Ferrostatin-1, as determined by Hoechst 33342 and PI staining (Figure E). Similar results were observed for Erastin and FIN56 (data not shown).

Figure 1: Effect of the ferroptosis inducers RSL3, Erastin and FIN56 and ferroptosis inhibitors on MDA-MB-231 cells

(A)

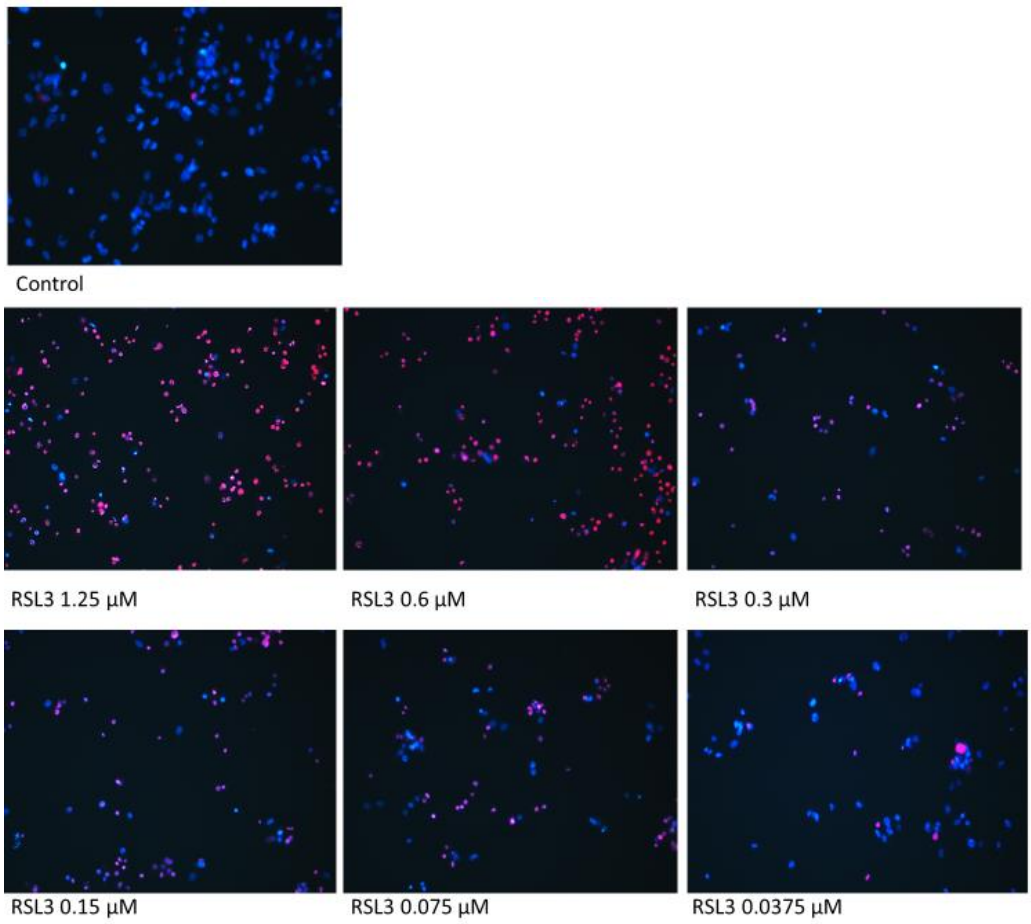

(B)

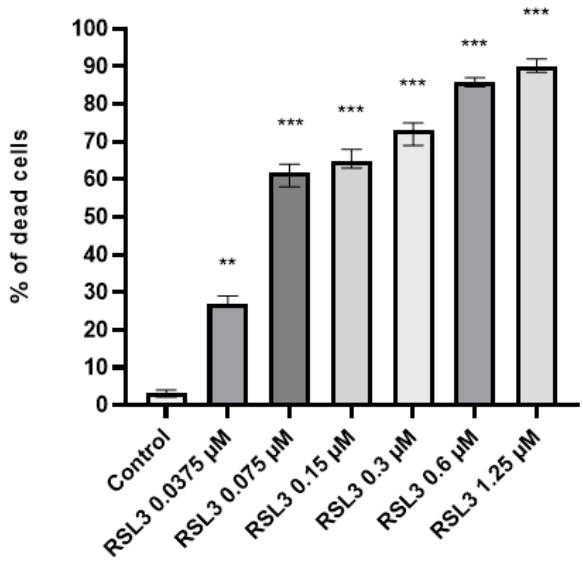

(C)

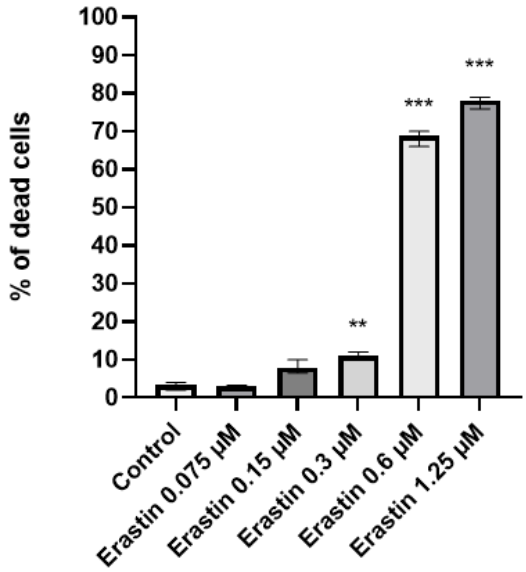

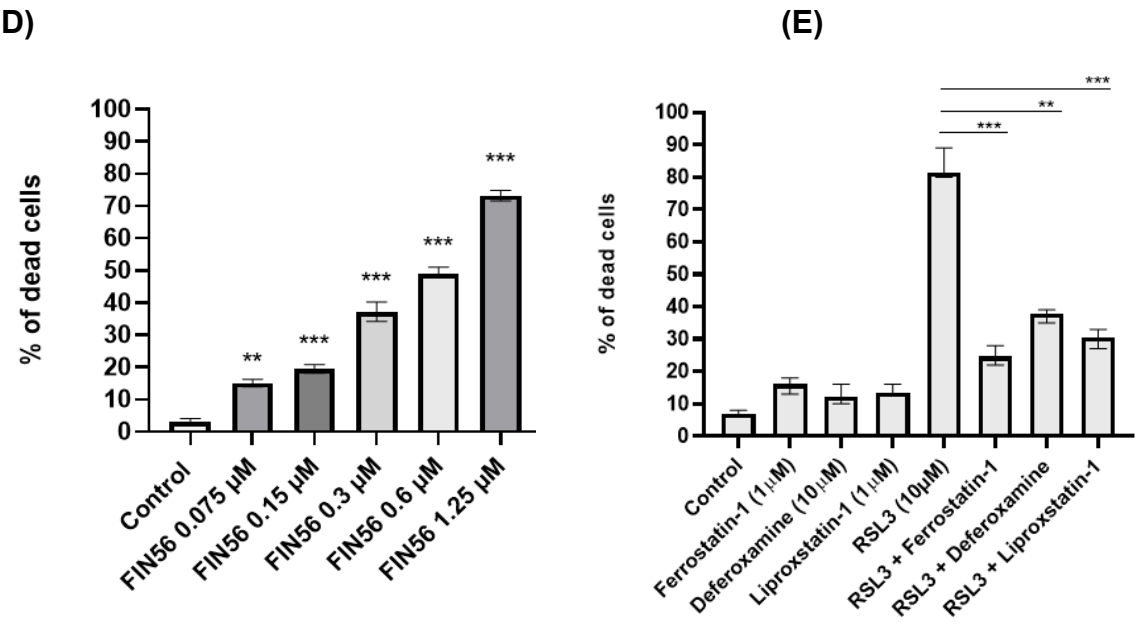

Figure 1: (A) Fluorescence microscopy analysis of cell death by Hoechst 33342/PI staining after treatment with the ferroptosis inducer RSL3 at concentration of 1.25, 0.6, 0.3, 0.15, 0.075 and 0.0375 µM. **(B-D).** Percentage of cell death calculated from 3 independent experiments each analysing triplicate wells for RSL3, Erastin and FIN56 respectively. **(E)** Reversal of ferroptosis after treatment with the ferroptosis inducer RSL3 (10 µM) +/- ferroptosis inhibitors (Deferoxamine 10 µM, Liproxstatin-1 1µM and Ferrostatin-1 1µM). Data is presented as median ± range. The statistical significance was determined by comparison with the control (0.2% (v/v) DMSO), analysed by a Kruskal-Wallis followed by Dunn's multiple comparisons test (*=P≤0.05, **=P≤0.01, and ***=P≤0.001).

The effect of ferroptosis inducers and inhibitors on MCF-7 cells

The ferroptosis inducers RSL3, Erastin and FIN56 at 10 µM showed no potent ferroptotic effect on MCF-7 cell death when compared to cells treated with the DMSO vehicle control (Figure 2). A 10 µM dose of each ferroptosis inducers was the highest dose that can reasonably be added to cells due its solubility in DMSO, and the potential cytotoxic effects of DMSO on cultured cells. This dose also killed almost all MDA-MD-231 cells, so similar 10 µM dose was used for all further experiments with MCF-7. The ferroptosis inhibitor Deferoxamine significantly induced ferroptosis when combined with the ferroptosis inducer RSL3 (P≤0.01), however all other ferroptosis inhibitors had little or no effect on MCF7 breast cancer cells.

Figure 2

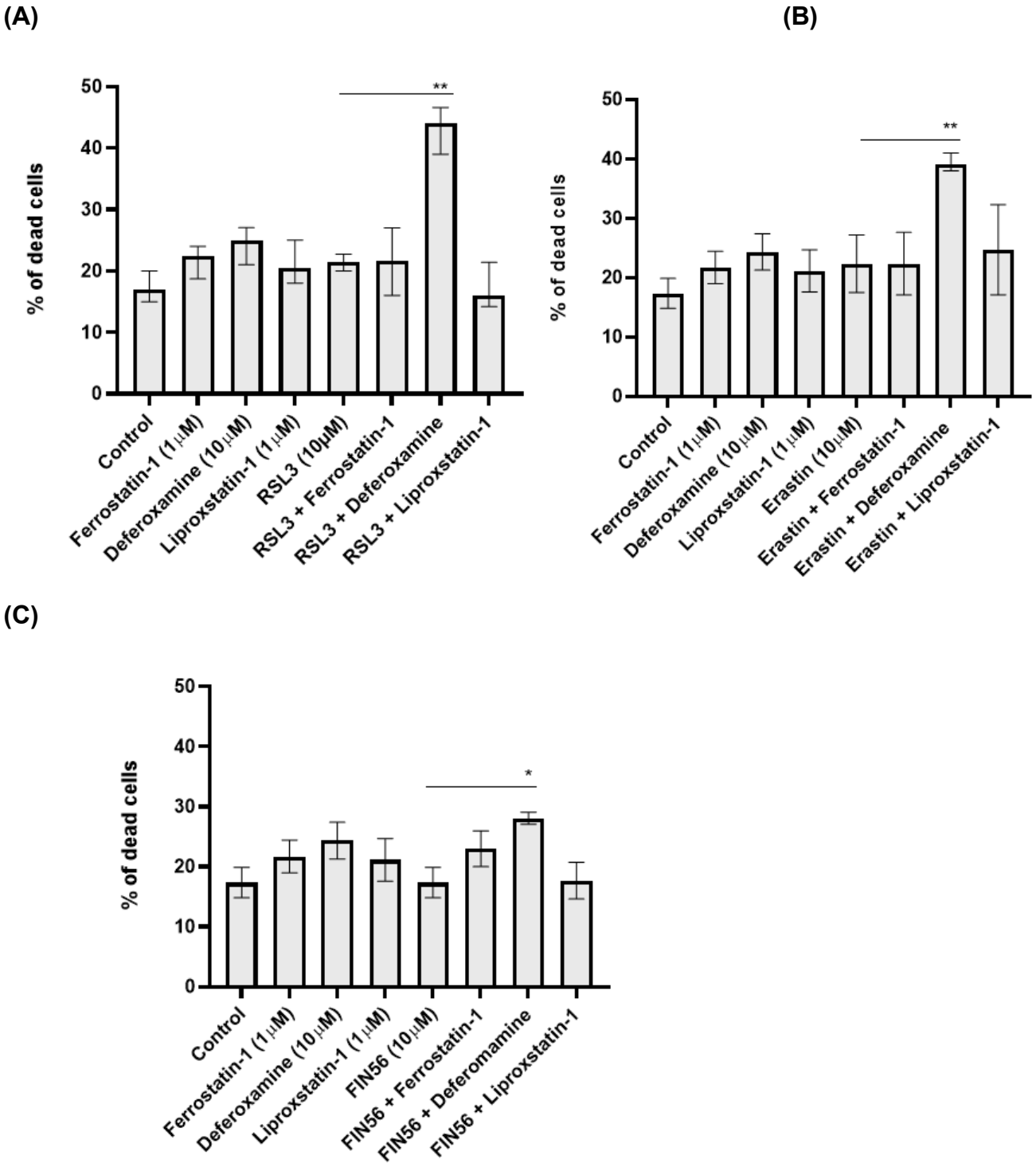

Figure 2: Fluorescence microscopy analysis of cell death by Hoechst 33342/PI staining after treatment with 10 μM of the ferroptosis inducers (A) RSL3, (B) Erastin and (C) FIN56, and the effects of ferroptosis inhibitors (Deferoxamine 10 μM, Liproxstatin-1 1μM and Ferrostatin-1 1μM). Data is presented as median ± range. The statistical significance was determined by comparison with the control (0.2% (v/v) DMSO), analysed by a Kruskal-Wallis followed by Dunn's multiple comparisons test (*=P≤0.05, **=P≤0.01, and ***=P≤0.001).

Effect of radiotherapy on colony formation in MDA-MB-231 and MCF-7 cells

Low dose of irradiation between 0 to 2.5 Gy were performed on the colony formation of MDA-MB-231 and MCF-7 cells grown in 2D cell culture (at a cell density of $10x10^3$ cells/well) and the percentage of colony survival was determined (Figure 3) in three technical repeats. For both cell lines, 1.25 Gy resulted approximately 60% reduction in colony formation over a 10–14-day period. Since this dose reduced colony formation over prolonged periods of time, it was presumed that this dose was inducting cell stress and was a suitable dose for shorter combination studies over 24-72 hours. This irradiation dose (1.25Gy) was used in all subsequent combination treatment regimes, with the ferroptosis inducers (Erastin, RSL3, FIN56) and the Nrf2 inhibitor ML385 in 2D cell culture following further optimization using CellTiter-Glo® luminescent cell viability assay to assess cytotoxicity over shorter time periods.

Figure 3 Colony formation assay of following irradiation

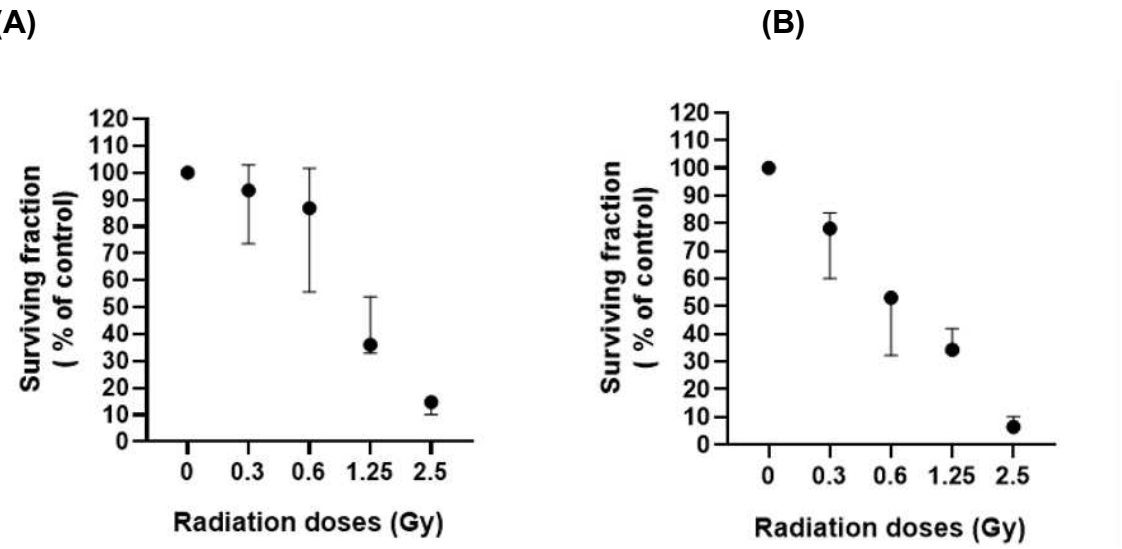

Figure 3: Cell survival of (A) MDA-MB-231 and (B) MCF-7 breast cancer cells grown in 2D, at a cell density of $1x10^3$ cells/wells. Following irradiation at 0 to 2.5 Gy cells were stained with crystal violet and the number of colonies formed were counted and compared to untreated control cells which were assigned a 100% survival rate. All treatment were repeated in triplicate and repeated in three technical repeats (n=3).

The effect of ferroptosis inducers on radiotherapy responses in MDA-MB-231 in 2D cell culture

To assess ferroptosis inducer-induced radiosensitivity, cells were treated with RSL3, Erastin or FIN56 for 72 hours immediately after irradiation with 1.25 Gy and stained with Hoechst 33342 and PI to assess cell death and apoptosis (Figure 4). Although colony formation assay showed potent effects of 1.25 Gy after 10-14 days, at shorter timepoints used for Hoechst 33342/PI staining, 1.25 Gy had only very modest effects on cell death. Since we knew that this dose must be having profound effects on the cells long-term, this dose was also used during short term irradiation treatments. Individual treatments did not significantly increase apoptosis or necrosis, but combined treatment did significantly increased cell death when compared to untreated control cells ($P \leq 0.05$), causing an additive effect with Erastin and FIN56 (Figure 4B-C). The data for cell death analysis using ferroptosis inducers-alone was consistent with the results obtained for ATP levels measured using 2D CellTiter-Glo® luminescent cell viability assay (Figure 4A-C), which showed a significant decrease in cell ATP levels after RSL3, Erastin, FIN56 or combination treatment vs. control. However almost all of these effects in combination treatments were due to the ferroptosis inducers. Erastin, RSL3 and FIN56 alone, caused a significant decrease in ATP levels when compared to control cells ($P \leq 0.001$). Importantly the ferroptosis inducer and irradiation combined treatment was not significant different from the use of ferroptosis inducer alone. This suggests that the majority of reduction in cell ATP levels in combination treatment was due to ferroptosis inducers, and there was no synergistic enhancement by irradiation (Figure 4).

Figure 4 The effect of ferroptosis inducers on radiotherapy responses in MDA-MB-231 in 2D cell culture

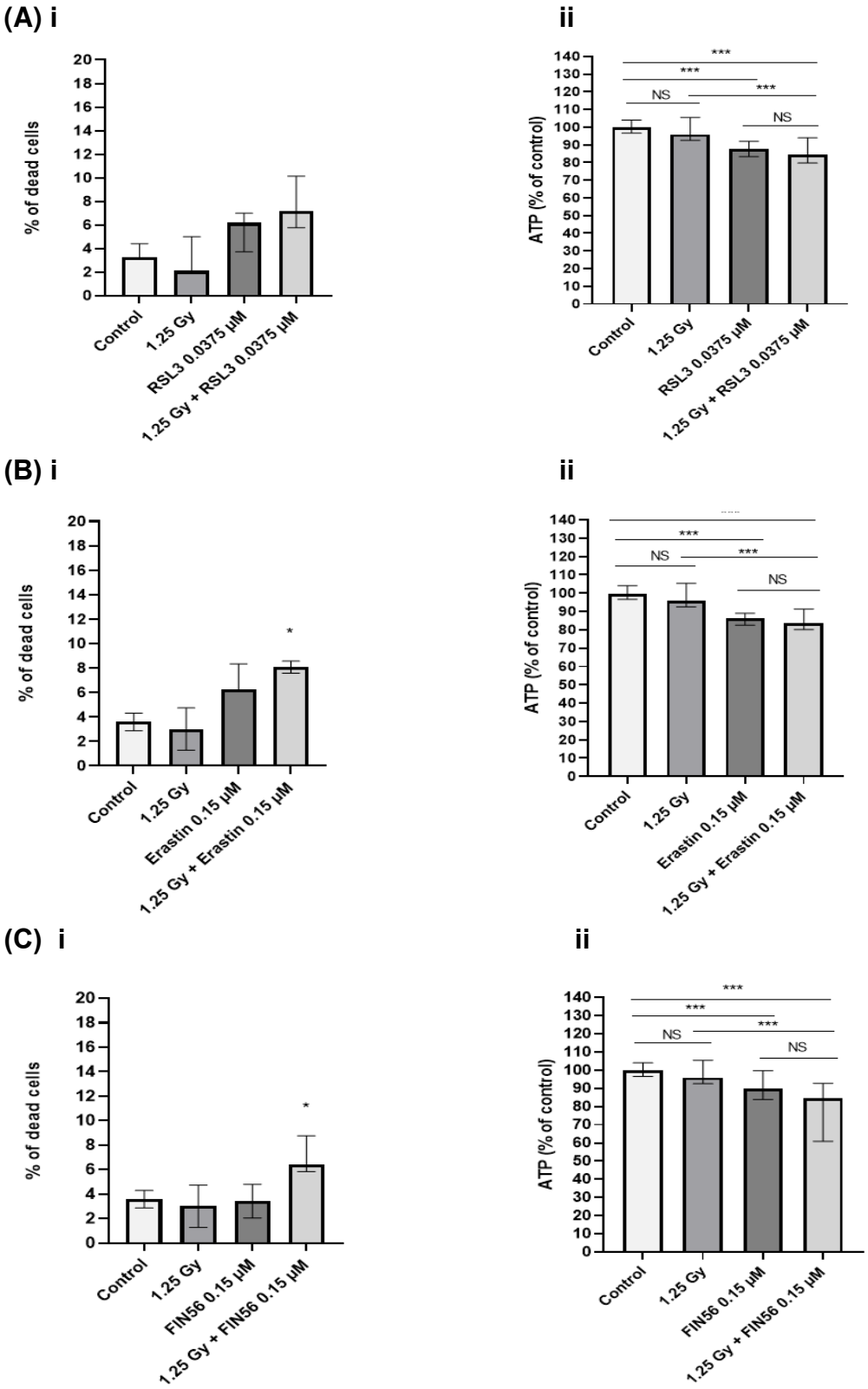

Figure 4. MDA-MB-231 cell line were treated with 1.25 Gy of radiation and the ferroptosis inducers (A) RSL3 (0.0375 µM, (B) Erastin (0.15 µM) or (C) FIN56 (0.15 µM) for 72 hours. Assessment of cell death following Hoechst 33342/PI staining was performed and data expressed as percentage of cell death (i), and assessment was made of cell ATP levels using the CellTiter-Glo® luminescent cell viability assay (ii). Data was normalised to the vehicle control which was

assigned 100% ATP levels. Data is presented as median ± range. All treatment were repeated in triplicate and repeated in three technical repeats (n=3). The statistical significance was determined by comparison with the control (0.2% (v/v) DMSO), analysed by a Kruskal-Wallis followed by Dunn's multiple comparisons test (*=P≤0.05, **=P≤0.01, and ***=P≤0.001).

The effect of ferroptosis inducers on radiotherapy responses in MCF-7 in 2D cell culture

To assess ferroptosis inducer-induced radiosensitivity, MCF-7 cells were treated with RSL3, Erastin or FIN56 for 72 hours immediately after irradiation and stained with Hoechst 33342 and PI to assess the percentage of cell death and apoptosis and ATP levels (Figure 5). RSL3 showed activity at the 72-hour time point, unlike at 24 hours, hence 0.6 µM dose used, and higher cell death observed for all ferroptosis inducers vs. Figure 2. RSL3, Erastin or FIN56 did not synergistically enhance responses to irradiation and combination treatments were not significantly different from RSL3, Erastin or FIN56-alone treatments (Figure 5).

Figure 5 The effect of ferroptosis inducers on radiotherapy responses in MCF-7 in 2D cell culture

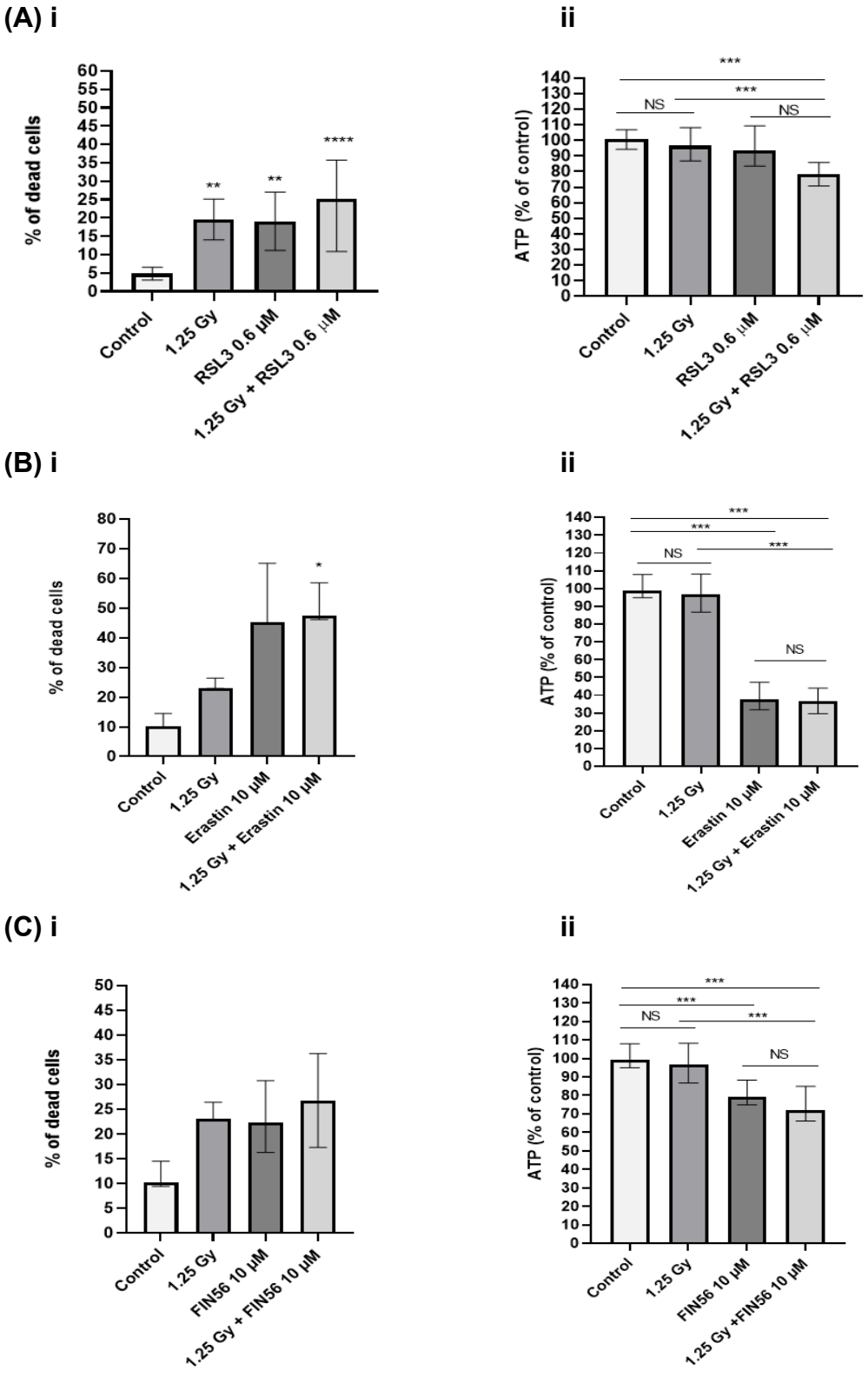

Figure 5. MCF-7 cells were treated with 1.25 Gy of radiation and the ferroptosis inducers (A) RSL3 (0.0375 µM), (B) Erastin (0.15 µM) or (C) FIN56 (0.15 µM) for 72 hours. Assessment of cell death following Hoechst 33342/PI staining was performed and data expressed as percentage of cell death (i) and assessment was made of cell ATP levels using the CellTiter-Glo® luminescent cell viability assay. Data was compared to the vehicle control (0.1% v/v DMSO) which was assigned 100% ATP levels. Data is presented as median ± range. All treatment were repeated in

triplicate and repeated in three technical repeats (n=3). The statistical significance was determined by comparison with the control (0.2% (v/v) DMSO), analysed by a Kruskal-Wallis followed by Dunn's multiple comparisons test (*=P≤0.05, **=P≤0.01, and ***=P≤0.001).

Effect of ferroptosis inducer RSL3 on radiotherapy responses in breast cancer 3D alginate spheroid cells

To assess RSL3-induced radiosensitivity, 3D alginate spheroids were treated with RSL3 for 72 hours immediately after irradiation with 20 Gy and stained with Hoechst 33342 and PI to assess cell death and apoptosis in MDA-MB-231 and MCF-7 cells (Figure 6 and 7 respectively). 20 Gy was chosen, as in parallel studies, 20 Gy induced cell death in some cell lines grown in alginate spheroids after 24 hours, whereas no cell death was observed at doses below 20 Gy (data not shown). Individual treatments and combined treatments did not significantly increase apoptosis or necrosis when compared to untreated controls, with the only exception being with RSL3 treated in MCF-7 cells. Here the Hoechst 33342 and PI staining showed different responses of treatments within the 3D spheroids, which clearly show the heterogeneity of responses within populations, in that some spheroids were dead, but others were unaffected (Figure 5 and 6 respectively). Combination treatment showed no enhancement of radiotherapy responses, despite single treatments of 20Gy being used; a dose that normally would cause kill all colonies after 14 days in a colony formation assay.

Figure 6 Combination treatment of RSL3 +/- radiotherapy in MDA-MB-231 3D alginate spheroids

(A)

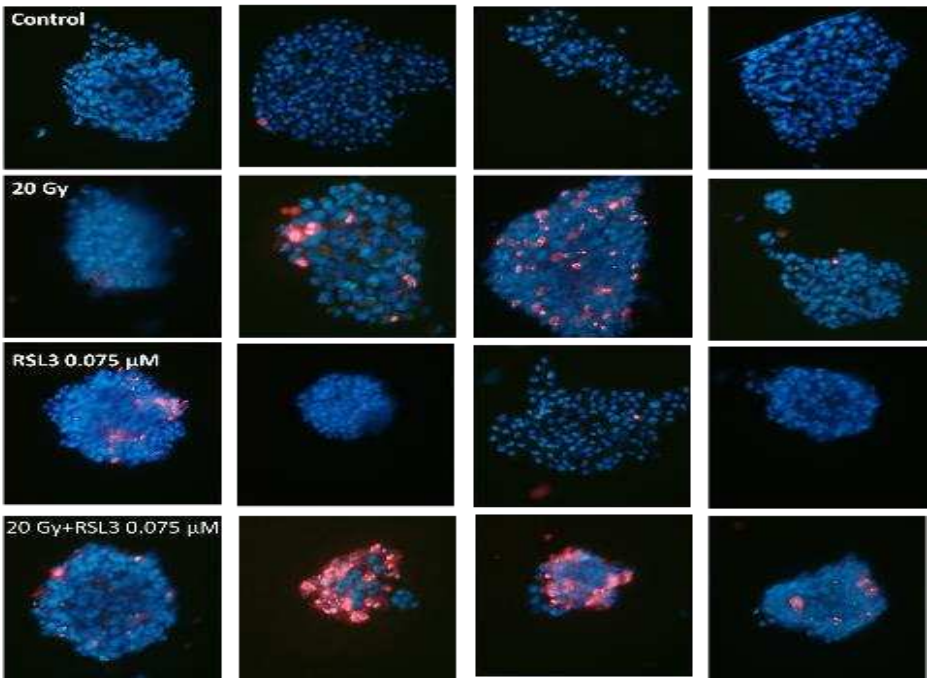

(B)

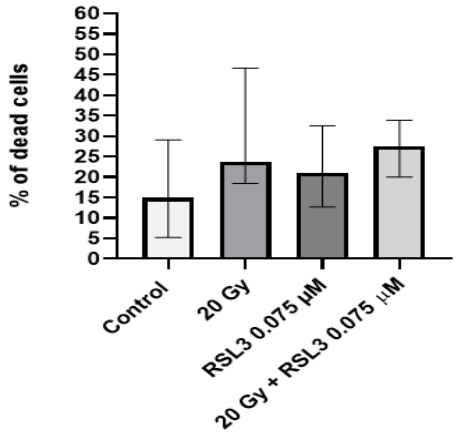

(C)

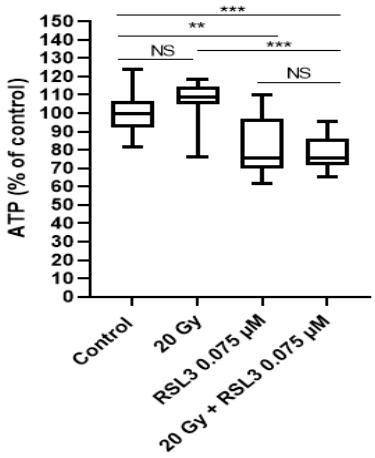

Figure 6. (A) Hoechst 33342/PI stained MDA-MB-231 spheroids treated with the vehicle control (0.2% (v/v) DMSO), 20 Gy radiation with and without the ferroptosis inducer RSL3 (0.075 µM). **(B)** Cell death count determined following Hoechst 33342/PI staining of MDA-MB-231 spheroids with radiation (20 Gy) and ferroptosis inducer RSL3 (0.075 µM), with a 0.2% (v/v) DMSO vehicle control. Data expressed as median ± range. **(C)** Percentage ATP levels of MDA-MB-231 spheroids level assessed by Cell Titer-Glo® 3D cell viability assay, following treating with radiation (20 Gy) and ferroptosis inducer RSL3 (0.075 µM). ATP levels were expressed as a percentage of the vehicle control (0.2% (v/v) DMSO) which was assigned a 100%. Data expressed as median ± interquartile range. All treatments were repeated in triplicate, in 4 or more technical repeats. The statistical significance was determined by comparison with the control (0.2% (v/v) DMSO), analysed by a Kruskal-Wallis followed by Dunn's multiple comparisons test (*=P≤0.05, **=P≤0.01, and ***=P≤0.001).

Figure 7 Combination treatment of RSL3 +/- radiotherapy in MCF-7 3D alginate spheroids

(A)

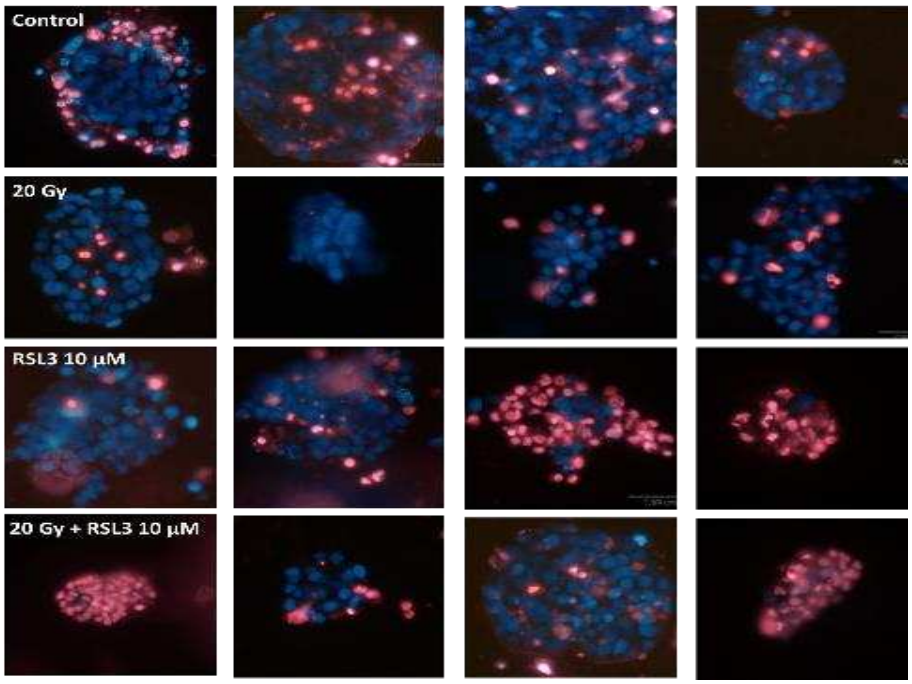

(B)

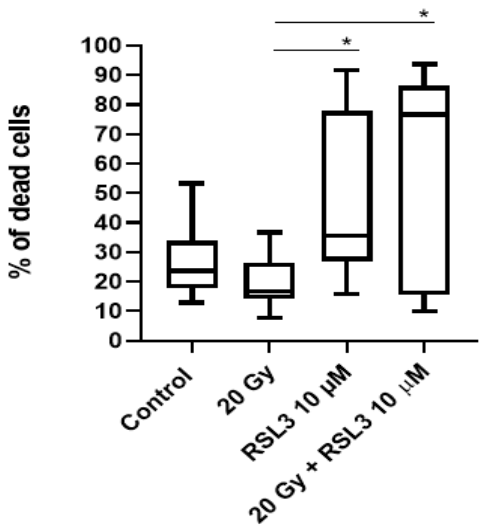

(C)

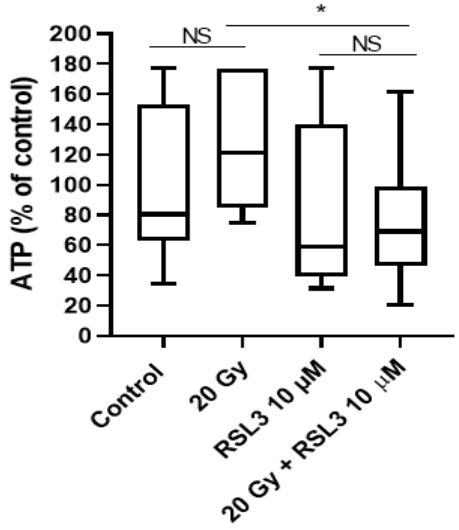

Figure 7: (A) Cell death was detection by fluorescent microscopy determined by Hoechst 33342/PI staining after treating MCF-7 spheroids with 20 Gy radiation, with control (0.2% (v/v) DMSO) +/- ferroptosis inducer RSL3 (10 µM). Median and interquartile ranges are shown in **(B). (C)** ATP level (% of control) assessed by Cell Titer-Glo® 3D Cell Viability Assay after treating MCF-7 spheroids with radiation (20 Gy) and ferroptosis inducer RSL3 (10 µM), with control (0.2% (v/v) DMSO). Data expressed as median ± interquartile range from n=3 independent experiments each with ≥4 technical repeats. The statistical significance was determined by comparison with the control (0.2% (v/v) DMSO), analysed by a Kruskal-Wallis followed by Dunn's multiple comparisons test (*=P≤0.05, **=P≤0.01, and ***=P≤0.001).

Immunocytochemistry to detect Nrf2 in breast cancer cells

Ferroptosis is controlled in part by the antioxidant response pathway, with is largely regulated by Nrf2, a transcription factor that binds to the promoter and induces transcription of many genes responsible for preventing ROS-induced cell stress, such as those resulting in glutathione synthesis. Prior to treatment with the Nrf2 inhibitor ML385, the basal levels of Nrf2 protein were assessed. Untreated 2D MDA-MB-231 and MCF-7 cells were stained with immunocytochemistry stain to localize the present of Nrf2 within cells. In MDA-MB-231, cells the distribution of Nrf2 was noticed in the nucleus, but signal was quite weak (Fingure 8A). In MCF-7 cells, the distribution of Nrf2 was seen more strongly in the nucleus (Figure 8B).

Figure 8. Nrf2 detection in breast cancer cells by immunocytochemistry

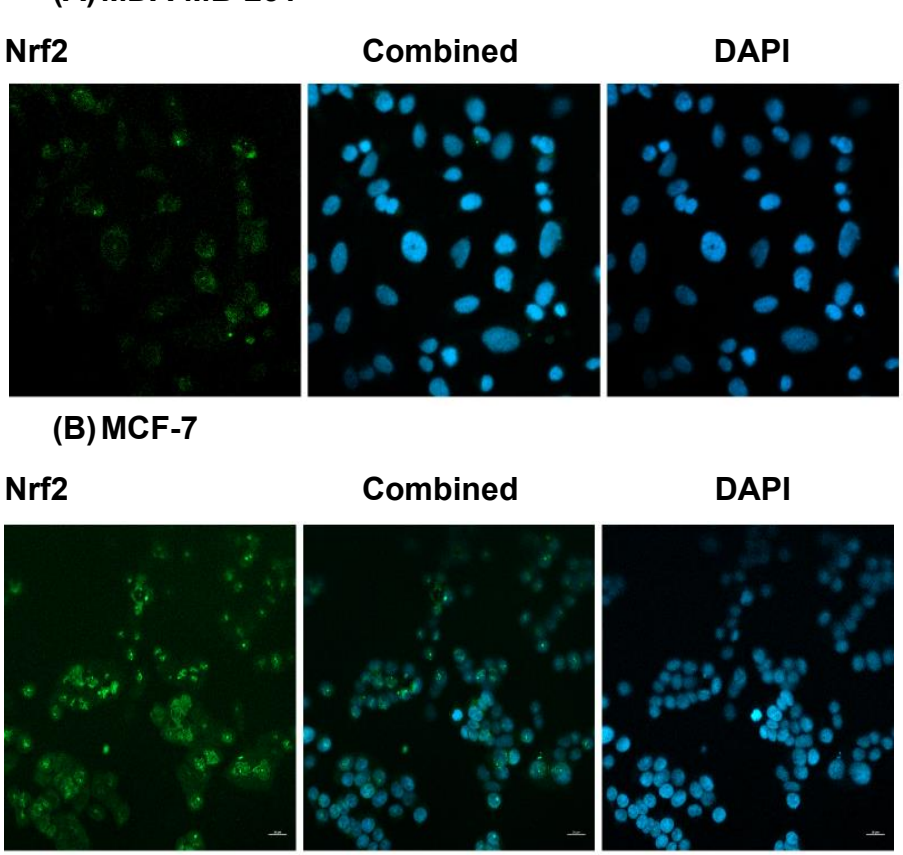

Figure 8 (A) MDA-MB-231 and (B) MCF-7 cells were stained for Nrf2 using the anti-human Nrf-2 antibody diluted visualized with an AlexaFluor 488-conjugated secondary antibody. Nuclei were counter stained with DAPI. Images were photographed using confocal fluorescence microscopy.

The effect of combination treatment of Nrf2 inhibitor ML385 alone and in combination with radiotherapy in breast cancer cells

To assess ML385-inhibitor mediated radiosensitivity, MDA-MB-231 and MCF-7 breast cancer cells were treated with ML385 for 72 hours immediately after irradiation and stained with Hoechst 33342 and PI to assess cell death and apoptosis (Figure 9). ML385 alone significantly increases

cell death (P≤0.05), and combined treatment significantly increased cell death when compared to the vehicle control in MDA-MB-231 cells (P≤0.05). However, this was clearly due to the ML385 alone, as only an effect rather than synergistic effect, when ML385 was used in combination with irradiation. The percentage ATP levels, following combined treatments were significantly reduced compared to the vehicle control (P≤ 0.001). Likewise, ML385 alone, and in combination irradiation when compared to vehicle control was significantly reduced (P≤0.001 for both). However, when the ML385/radiotherapy combination was compared to ML385 alone, there was not significantly difference in cell ATP levels. Therefore, cell death and reductions in cell ATP levels following ML385 treatment was not enhanced by irradiation (Figure 9).

In MCF-7 cells, ML385 alone significantly increase cell death (P≤0.05), and combined treatment significantly increased cell death vs. control (P≤0.05) (Figure 10AB), however this was clearly due to the ML385. Assessment of ATP levels showed a similar effect. The ML385/irradiation combination treatments and ML385 alone significantly decreased ATP levels compared to the vehicle control (P≤0.001 for both); but once again the ML385/irradiation combination treatments were not significantly different form the ML385 treatment alone (P≤0.001), suggesting that the majority of cell death and reduction in ATP levels could be contributed to ML385, and there was no enhancement in the effect of irradiation (Figure 10C).

Figure 9. The effect of combination treatment of Nrf2 inhibitor ML385 +/- radiotherapy in MDA-MB-231 cells

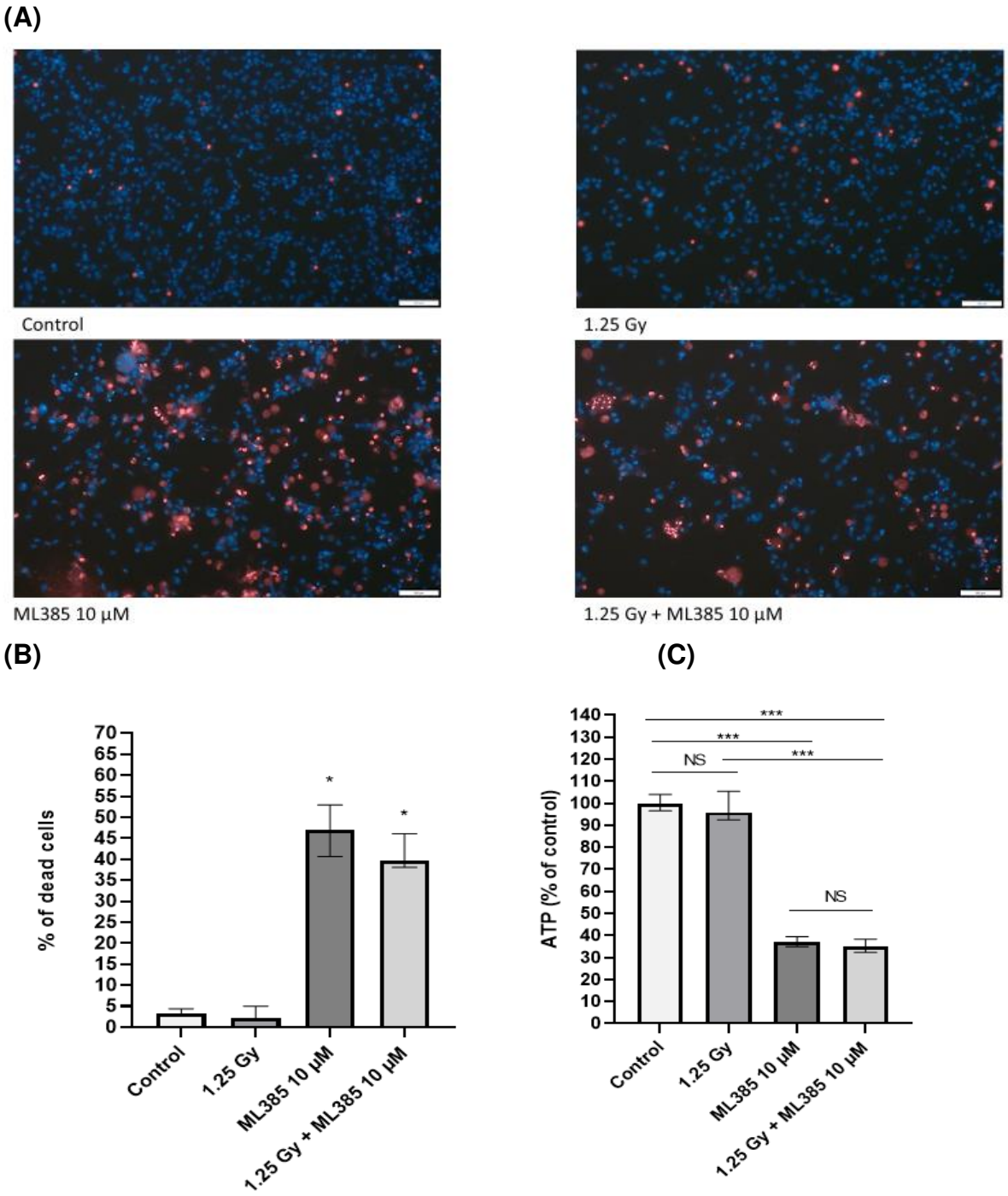

Figure 9: (A) Cell death was determined by Hoechst 33342/PI staining under fluorescent microscopy after treating MDA-MB-231 cells with 1.25 Gy radiation, +/- ML385 (10 µM). Live cells and apoptotic cells are stained blue with Hoechst 33342, dead cells are stained red with PI staining. **(B)** Cell death count determined by Hoechst 33342/PI staining **(C)** ATP level (% of control) assessed by CellTiter-Glo® luminescent cell viability assay after treating MDA-MB-231 cell line with radiation (1.25 Gy) and ML385 (10 µM), with control (0.2% (v/v) DMSO). All treatment were repeated in triplicate and repeated in three technical repeats (n=3). The statistical significance was determined by comparison with the control (0.2% (v/v) DMSO), analysed by a Kruskal-Wallis followed by Dunn's multiple comparisons test (*=P≤0.05, **=P≤0.01, and ***=P≤0.001).

Figure 10. The effect of combination treatment of Nrf2 inhibitor ML385 +/- radiotherapy MCF-7 cells

(A)

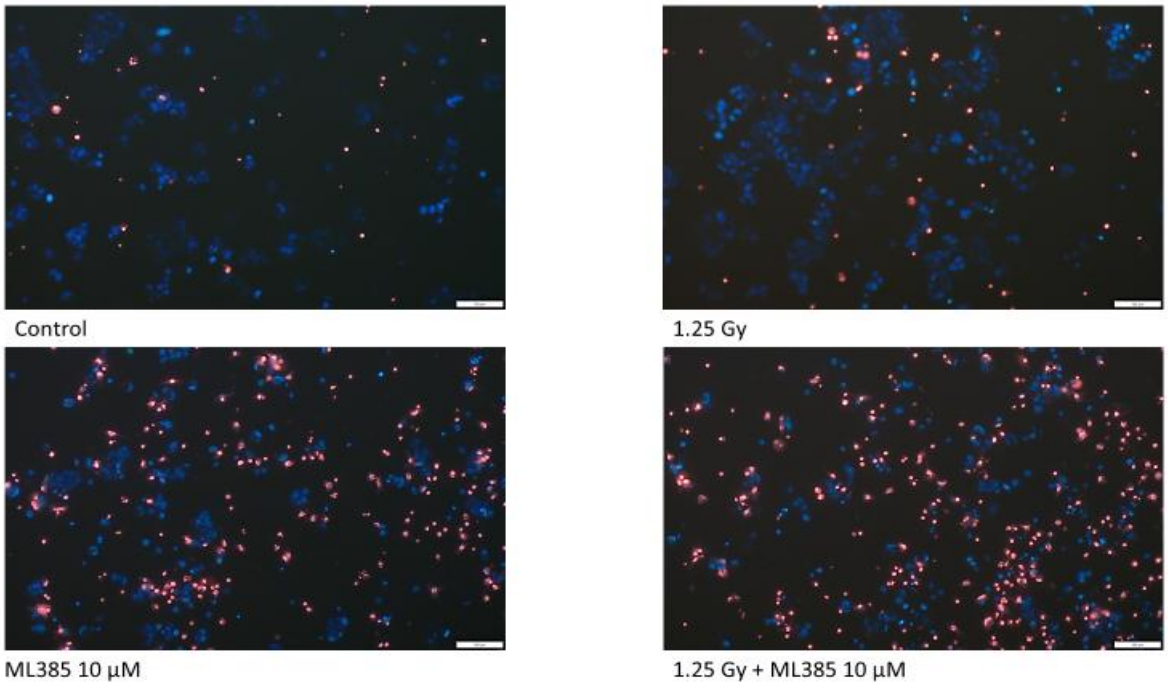

(B)

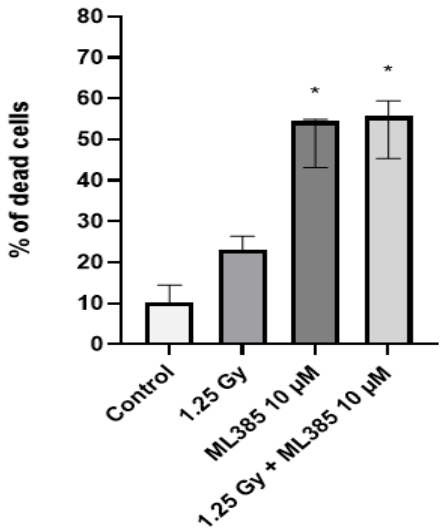

(C)

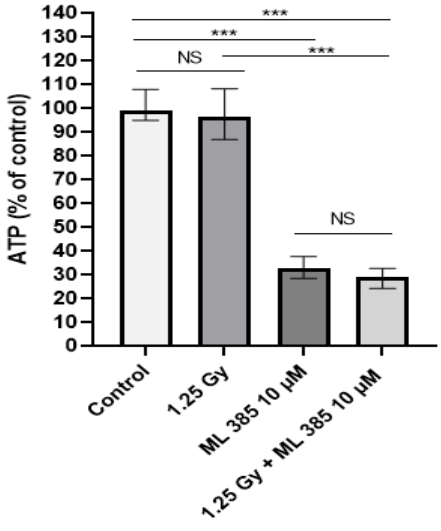

Figure 10. (A) Cell death was detected by fluorescent microscopy by Hoechst 33342/PI staining after treating MCF-7 cell line with 1.25 Gy radiation +/- ML385 (10 µM). Live cells cells are stained blue with Hoechst 33342, dead cells are stained red with PI staining. **(B)** Cell death count determined by Hoechst 33342/PI staining after treating MCF-7 cell line with radiation (1.25 Gy) and ML385 (10 µM). **(C)** ATP level (% of control) assessed by CellTiter-Glo® luminescent cell viability assay after treating MCF-7 cell line with radiation (1.25 Gy) and ML385 (10 µM), with control (0.2% (v/v) DMSO). All treatment were repeated in triplicate and repeated in three technical repeats (n=3). The statistical significance was determined by comparison with the control (0.2% (v/v) DMSO), analysed by a Kruskal-Wallis followed by Dunn's multiple comparisons test (*=P≤0.05, **=P≤0.01, and ***=P≤0.001).

Effect of Nrf2 inhibitor on radiotherapy responses in breast cancer 3D alginate spheroid cells

To assess the therapeutic potential of the Nrf2 inhibitor ML385, 3D alginate spheroids were treated with ML385 for 72 hours immediately after irradiation, they were then stained with Hoechst 33342 and PI to assess cell death (Figure 11AB). The percentage of cell death observed following individual ML385 or radiation treatments were not significantly different, however the use of ML385 treatment alone did significantly increased cell death when compared to the vehicle control ($P \leq 0.05$). There was no significant increase in cell death when radiation treatment was and combined with ML385.

Assessment of cell ATP levels showed that ATP levels were significantly reduced following ML385 and radiation combined treatments when compared to the vehicle to control ($P \leq 0.01$), but ML385 alone when compared to vehicle control did significantly reduce cell ATP levels ($P \leq 0.001$). Combined treatment of ML385 with radiotherapy ($P \leq 0.001$) when compared to ML385 alone were not significantly different to each other. This suggested that the majority of reduction in ATP level in combination treatment was due to ML385, and there was no enhancement by radiotherapy (Figure 11C).

Figure 11. Combination treatment of ML385 +/- radiotherapy in MDA-MB-231 3D alginate spheroids

(A)

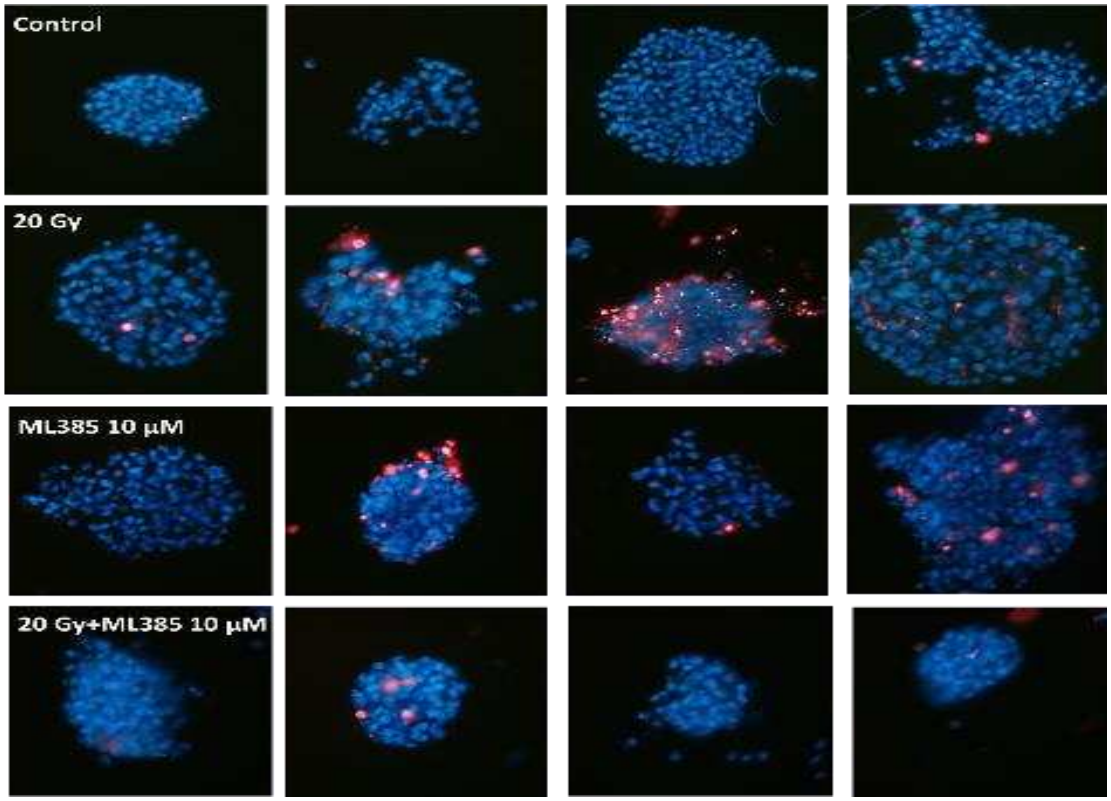

(B) **(C)**

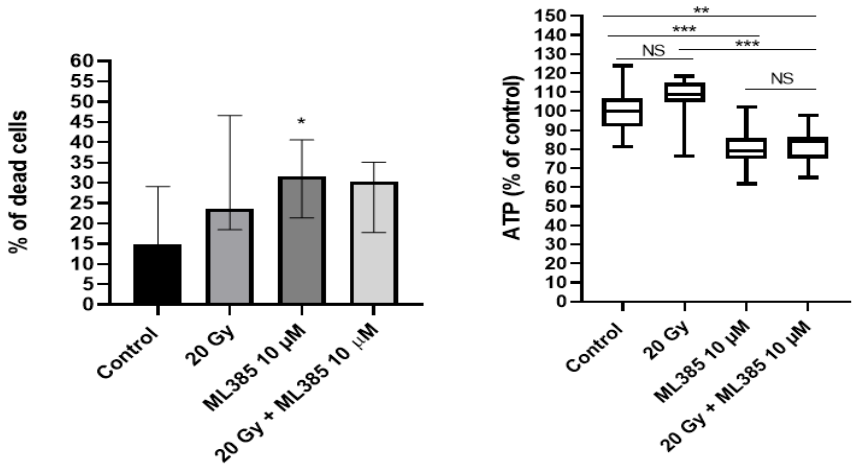

Figure 11: (A) Cell death was determined by Hoechst 33342/PI staining after treating MDA-MB-231 spheroids with 20 Gy radiation +/- the Nrf2 inhibitor ML385 (10 µM), **(B)** Cell death count determined by Hoechst 33342/PI staining after treating MDA-MB-231 spheroids with radiation (20 Gy) and ML385 (10 µM). Data expressed as median ± range. **(C)** ATP level (% of control) assessed by Cell Titer-Glo® 3D cell assay after treating MDA-MB-231 spheroids with radiation (20 Gy) and ML385 (10 µM), with control (0.2% (v/v) DMSO). Data expressed as median ± interquartile range from n=3 independent experiments each with ≥4 technical repeats. The statistical significance was determined by comparison with the control (0.2% (v/v) DMSO), analysed by a Kruskal-Wallis followed by Dunn's multiple comparisons test (*=P≤0.05, **=P≤0.01, and ***=P≤0.001).

Discussion

The aim of this study was to assess whether radiotherapy responses could be enhanced in 2D and 3D cell cultures of breast cancer cells. To assess this, MDA-MB-231 and MCF-7 cells were treated with ferroptosis inducers and Nrf2 inhibitors after radiotherapy and assessed by direct assessment of cell death, and by measurements of ATP as a marker of cell viability. In summary, in these studies, MCF-7 and MDA-MB-231 breast cancer cells do not show enhanced radiosensitivity when treated with either ferroptosis inducers, or a Nrf2 inhibitor.

Colony formation assays were performed on breast cancer MDA-MB-231 and MCF-7 cells to initially optimize the doses of radiation. There was a relationship between colony numbers and radiation dose. The optimal radiation dose for colony assays for 2D cells was 1.25 Gy, and this was used for direct cell death experiments using Hoechst 33342/PI, and an assessment of cell ATP levels. The rationale for this was that ferroptosis is a relatively fast cell death mechanism, and although colony formation measures the number of cells able to actively proliferate over a period of up to 2 weeks, in-part in response to DNA repair being successfully resolved, we were specifically interested in immediate effects of ferroptosis enhancement.

Ferroptosis inducers did not enhance radiotherapy effects in 2D cell culture

Both MCF-7 and MDA-MB-231 were irradiated and then immediately treated with doses of RSL3, Erastin or FIN56 at doses that were known to induce cell death in a minority of cells, but not induce high levels of cell death. In all cases, there was no consistent synergistic response in combination treatment. In only FIN56 treatment of MDA-MB-231 showed evidence of a very weak effect when combined with irradiation (Figure 4C). In all cases, ATP levels generally followed cell death observations with no synergistic responses seen.

There is evidence to suggest that ferroptosis inducers such as Erastin may enhance the sensitivity of cancer cells to radiotherapy (Ye *et al.*, 2020). Erastin inhibits system Xc- reducing cysteine import and hence decreased glutathione, meaning there is less glutathione to respond to irradiation-induced ROS. In addition, some studies have suggested that ferroptosis may play a role in the radiosensitivity of cancer stem cells (Cosialls *et al.*, 2021; Liu *et al.*, 2022), which are thought to be responsible for cancer recurrence and resistance to radiotherapy. On the other hand, cancer cells after radiation may evade cell death via modulation of ferroptosis by several mechanisms. In the presence of a Keap-1 mutation, Nrf2 is high, leading to an enhanced antioxidant response. Irradiation-mediated ROS may have little effect in this situation. Similarly, Acyl coenzyme A synthetase long chain family member 4 (ACLS4) is low in some breast cancers, this is primarily responsible for catalysing the conversion of free PUFAs such arachidonic acids (AAs) and adrenic acids (AdAs) to their acyl coenzyme A (CoA) derivatives, such as AA/AdA-

CoA. These PUFA-CoAs are then converted into lysophospholipids (LysoPLs), which are then further incorporated into phospholipids (such AA-PE and AdA-PE) by lysophosphatidylcholine acyltransferase 3 (LPCAT3) and other enzymes. Hence, PUFA-PL synthesis is suppressed and ferroptosis resistance is markedly increased when ACSL4 or LPCAT3 are suppressed (Dixon *et al*, 2015, Doll *et al*, 2017). This was supported by other studies of radioresistant sublines of MCF-7 cells, which were showed a loss of ACSL4 (Kwon *et al*, 2021). Furthermore, ASCL4 is essential for mediating radiation-induced damage in normal tissues, and specific ASCL4 inhibitors are being trialled as inhibitors of ferroptosis-induced radiation damage (Ji *et al,* 2022).

The major ferroptosis defence system is thought to be the solute carrier family 7 member 11-glutathione-GPX4 (SLC7A11-GSH-GPX4) signalling axis; in fact, ferroptosis was first discovered due to experiments on this signalling axis (Dixon *et al,* 2012, Yang *et al,* 2014). A crucial part of the cystine/glutamate antiporter system Xc^-, SLC7A11, facilitates the antiporter action of system Xc^- by bringing in extracellular cystine and releasing intracellular glutamate (Koppula *et al,* 2018). Irradiation is known to increase SLC7A11 expression, leading to increased cystine uptake and increased GSH production, resulting in a reduced response to radiation (Koppula *et al,* 2021) and therefore SLC11A7 overexpression leads to radio-resistance (Xie et al, 2011, Lei *et al,* 2020), whereas decreased SLC11A7 leads to radiosensitivity (Cobler *et al,* 2018, Nagane et al, 2018, Lei *et al,* 2020). According to Koppula *et al.* (2018), after extracellular cystine is taken up by SLC7A11, it is immediately reduced to cysteine in the cytosol through a reduction mechanism that consumes NADPH. Next, as a key cofactor for GPX4 to detoxify lipid peroxides, cysteine acts as the rate-limiting precursor for the manufacture of GSH (Koppula *et al*., 2021). Many cancer cells undergo significant ferroptosis when SLC7A11 transporter activity is blocked or when cystine is not present in culture media (Koppula *et al,* 2021). Importantly, some tumour suppressors, including p53, BAP1, ADP-ribosylation factor (ARF), and Kelch-like ECH-associated protein 1 (KEAP1), induce ferroptosis by inhibiting the production or function of SLC7A11 (Jiang *et al,* 2015, Zhang et al, 2018). Similarly, by binding to the SLC7A11 promoter, activating transcription factor 3 (ATF3) suppresses SLC7A11 expression and increases the vulnerability of cancer cells to ferroptosis (Wang *et al,* 2020). Nrf2 and activating transcription factor 4 (ATF4) are examples of stress-responsive transcription factors that can promote SLC7A11 under a variety of stress circumstances, including oxidative stress and amino acid deficiency, protecting cells from ferroptosis (Habib *et al,* 2015). Therefore, SLC7A11 is an endogenous protective protein against radiation induced damage in normal cells, which can be exploited immediately after radiotherapy by tumour cells and can be over-expressed in tumour cells to generate an intrinsically radioresistant phenotype.

Nrf2 inhibition did not enhance radiotherapy effects.

The Nrf2 inhibitor, ML385 was combined with the optimized levels of radiation of 1.25 Gy for 2D and 20 Gy for 3D and the result of ATP levels and cell death using Hoechst 33342/PI staining show no enhancement of radiation responses in both MDA-MB-231 and MCF-7 breast cancer cell lines at 72 hours. Since ML385 is a direct inhibitor of Nrf2, it was hypothesised that ML385 would attenuate the Nrf2-mediated antioxidant response which becomes activated after irradiation and increases cell death. Despite Nrf2 expression being much higher in MCF-7 cells than MDA-MB-231, with increased nuclear Nrf2 in MCF-7 (Figure 8), both cell lines responded similarly to ML385 alone suggesting that in standard growth conditions, cells are dependent on Nrf2-mediated antioxidant response to survive. In both cases, combination of ML385 and ML385 + radiotherapy resulted in essentially no difference in cell death, either by ATP measurements or Hoechst 33342/PI staining. The reason for this is unclear. Cells were treated with ML385 within 2 hours of irradiation which may be a factor. Further experiments with either pre-treatment, or post-treatment are required. It is possible that the Nrf2 pathway does not play a significant role in the radiation response in breast cancer cells or that ML385 causes the activation of alternative compensatory mechanisms. However, it is important to note that ML385 may have the ability to make other cancer cells more susceptible to radiation therapy in other tumour models, such as lung cancer (Singh *et al,* 2020). Furthermore, the formation of ROS and DNA damage are two factors that affect radiotherapy effectiveness. Excessive ROS production can cause cell death or activate defence mechanisms like the Keap1/Nrf2 pathway, which controls intracellular cysteine availability by upregulating SLC7A11, a subunit of the system Xc^- transporter, and subsequently glutathione synthesis, enhancing antioxidative defence (Bader *et al,* 2021). In various cancer cell lines, Nrf2, a transcription factor that promotes the expression of genes containing antioxidant response elements (ARE), has been linked to providing resistance to chemotherapy and presumably radiotherapy also as both are associated with cell death mechanisms that are ROS-dependent (Roh *et al,* 2017).

Cells grown in as 3D alginate spheres are intrinsically radio-resistant

Cells grown in 3D alginate spheres showed limited radiosensitivity at 20 Gy, whereas at this dose, almost all cells were killed in 2D colony formation assays. The reasons for this are unclear but observations supported by other researchers and results mirror chemotherapy responses. The radio-resistance of breast cancer cells could be due the capability of cancer cells to protect themselves from excess ROS. It is known that cells in 3D cell culture experience increased ROS, and induce Nrf2 in the hypoxic core, and that Nrf2 expression is a pre-requisite for sphere formation (Takahashi *et al,* 2020). Ionizing radiation damages DNA directly or indirectly by

radiolyzing water, producing ROS and causing additional oxidative stress-related damage to biomolecules. Tumour cells evolve defence systems to prevent cell death due to repeated ROS exposure, and gain of Nrf2, or in the case of some breast cancers loss of Keap-1, allows clonal evolution of surviving Nrf2-high cells (Takahashi *et al,* 2020). These Nrf2-dependent mechanisms enhance DNA repair and boost anti-oxidation defence, neutralising ROS, reducing oxidative stress, and limiting ROS-induced damage (Bader *et al,* 2021).

Another reason of radioresistant according to the "oxygen fixation hypothesis" and the activation of hypoxia-inducible factors (HIFs), the hypoxic tumour microenvironment is a significant radio-resistance mechanism (Wang *et al,* 2019). And usually this occurs in 3D cell culture as a mimic of *in vivo* responses rather than 2D monolayer cells, because they mimic the tumour microenvironment (DelNero *et al,* 2015). On the other hand, hypoxia increases the production of ROS; as a result, hypoxic tumour cells heavily rely on antioxidant systems to maintain redox equilibrium, and GSH inhibition was demonstrated to overcome hypoxia-mediated radio-resistance (Wang *et al,* 2019). It is intriguing that HIFs (HIF-1 and -2) have been linked to ferroptosis susceptibility. Renal cancer cells are also more vulnerable to ferroptosis when HIF-1 is activated (Zuo *et al,* 2019).

Cells growth in 3D cell culture show heterogeneous ferroptosis responses.

Treating cells grown in 3D cell culture with the ferroptosis inducer RSL3 (Figures 9-10) and to some extent ML385 (Figure 11) showed that some colonies respond to treatment and die, while other colonies survive showing heterogeneity within these populations of tumour cells. Interestingly, a parallel phenomenon has very recently been described in TNBC whereby cancers show marked heterogeneity with respect to ferroptosis markers (Yang *et al,* 2023). Similarly, ferroptotic heterogeneity has also been reported in melanoma (Lin *et al,* 2022) which mirrors observations for heterogeneity of apoptosis inducers in breast cancer cells and other tumour cell types (Cross *et al,* 2008, Spencer *et al,* 2009). Further research is necessary to determine the possibility and precise processes by which ferroptosis activation and Nrf2 inhibition can decrease the radio-resistance of hypoxic cancer cells in various cancer situations, and to identify metabolic signatures of ferroptosis-sensitive vs. resistant populations.

Summary

MDA-MB-231 and MCF-7 cells were sensitive to irradiation in 2D cell culture but resistant to irradiation in 3D cell culture. After induction of cell death with ferroptosis inducers, there was no short-term robust enhancement to radiation effect to the breast cancer cells either in 2D or 3D cell culture. The Nrf2 inhibitor ML385 showed no further effect on radiotherapy. These studies suggest targeting ferroptosis does not induce short-term enhancement of ferroptotic cell death.

Further studies using pre-treatment of ferroptosis prior to radiotherapy are required, as well as studies using repeated fractionation of doses over a prolonged period of time to mimic the clinical situation, which is particularly relevant to treatment of 3D spheroids. Furthermore, these studies require repeating in standard colony formation assays to assess longer-term effects of combination treatments.

Acknowledgements

This study was funded by a PhD scholarship from the Kuwait Embassay Cultural Office.

References

Bader S, Wilmers J, Pelzer M, Jendrossek V, Rudner J. Activation of anti-oxidant Keap1/Nrf2 pathway modulates efficacy of dihydroartemisinin-based monotherapy and combinatory therapy with ionizing radiation. Free Radic Biol Med. 2021 168:44-54. doi: 10.1016/j.freeradbiomed.2021.03.024.

Baird L, Yamamoto M. The Molecular Mechanisms Regulating the KEAP1-NRF2 Pathway. Mol Cell Biol. 2020 40(13):e00099-20. doi: 10.1128/MCB.00099-20.

Cobler L, Zhang H, Suri P, Park C, Timmerman LA. xCT inhibition sensitizes tumors to γ-radiation via glutathione reduction. Oncotarget. 2018 9(64):32280-32297. doi: 10.18632/oncotarget.25794.

Cosialls E, El Hage R, Dos Santos L, Gong C, Mehrpour M, Hamaï A. Ferroptosis: Cancer Stem Cells Rely on Iron until "to Die for" It. Cells. 2021 10(11):2981. doi: 10.3390/cells10112981.

Cross NA, Waterman EA, Jokonya N, Fowles A, Buckle CH, Phillips J, Holen I, Hamdy FC, Eaton CL. Phenotypic variations of TRAIL sensitivity in cloned populations of prostate cancer cells. J Cell Biochem. 2008 104(4):1452-64. doi: 10.1002/jcb.21721.

DelNero P, Lane M, Verbridge SS, Kwee B, Kermani P, Hempstead B, Stroock A, Fischbach C. 3D culture broadly regulates tumor cell hypoxia response and angiogenesis via pro-inflammatory pathways. Biomaterials. 2015 55:110-8. doi: 10.1016/j.biomaterials.2015.03.035.

Dixon SJ, Lemberg KM, Lamprecht MR, Skouta R, Zaitsev EM, Gleason CE, Patel DN, Bauer AJ, Cantley AM, Yang WS, Morrison B 3rd, Stockwell BR. Ferroptosis: an iron-dependent form of nonapoptotic cell death. Cell. 2012 149(5):1060-72. doi: 10.1016/j.cell.2012.03.042.

Dixon SJ, Patel DN, Welsch M, Skouta R, Lee ED, Hayano M, Thomas AG, Gleason CE, Tatonetti NP, Slusher BS, Stockwell BR. Pharmacological inhibition of cystine-glutamate exchange induces endoplasmic reticulum stress and ferroptosis. Elife. 2014 3:e02523. doi: 10.7554/eLife.02523.

Dixon SJ, Winter GE, Musavi LS, Lee ED, Snijder B, Rebsamen M, Superti-Furga G, Stockwell BR. Human Haploid Cell Genetics Reveals Roles for Lipid Metabolism Genes in Nonapoptotic Cell Death. ACS Chem Biol. 2015 10(7):1604-9. doi: 10.1021/acschembio.5b00245.

Doll S, Proneth B, Tyurina YY, Panzilius E, Kobayashi S, Ingold I, Irmler M, Beckers J, Aichler M, Walch A, Prokisch H, Trümbach D, Mao G, Qu F, Bayir H, Füllekrug J, Scheel CH, Wurst W, Schick JA, Kagan VE, Angeli JP, Conrad M. ACSL4 dictates ferroptosis sensitivity by shaping cellular lipid composition. Nat Chem Biol. 201713(1):91-98. doi: 10.1038/nchembio.2239.

Dolma S, Lessnick SL, Hahn WC, Stockwell BR. Identification of genotype-selective antitumor agents using synthetic lethal chemical screening in engineered human tumor cells. Cancer Cell. 2003 3(3):285-96. doi: 10.1016/s1535-6108(03)00050-3

Feng Y, Madungwe NB, Imam Aliagan AD, Tombo N, Bopassa JC. Liproxstatin-1 protects the mouse myocardium against ischemia/reperfusion injury by decreasing VDAC1 levels and restoring GPX4 levels. Biochem Biophys Res Commun. 2019 520(3):606-611. doi: 10.1016/j.bbrc.2019.10.006.

Habib E, Linher-Melville K, Lin HX, Singh G. Expression of xCT and activity of system xc(-) are regulated by NRF2 in human breast cancer cells in response to oxidative stress. Redox Biol. 2015 5:33-42. doi: 10.1016/j.redox.2015.03.003.

He F, Ru X, Wen T. NRF2, a Transcription Factor for Stress Response and Beyond. Int J Mol Sci. 2020 21(13):4777. doi: 10.3390/ijms21134777.

Jiang L, Kon N, Li T, Wang SJ, Su T, Hibshoosh H, Baer R, Gu W. Ferroptosis as a p53-mediated activity during tumour suppression. Nature. 2015 520(7545):57-62. doi: 10.1038/nature14344.

Ji Q, Fu S, Zuo H, Huang Y, Chu L, Zhu Y, Hu J, Wu Y, Chen S, Wang Y, Ren Y, Pu X, Liu N, Li R, Wang X, Dai C. ACSL4 is essential for radiation-induced intestinal injury by initiating ferroptosis. Cell Death Discov. 20228(1):332. doi: 10.1038/s41420-022-01127-w.

Kamble D, Mahajan M, Dhat R, Sitasawad S. Keap1-Nrf2 Pathway Regulates ALDH and Contributes to Radioresistance in Breast Cancer Stem Cells. Cells. 2021 10(1):83. doi: 10.3390/cells10010083.

Koppula P, Zhang Y, Zhuang L, Gan B. Amino acid transporter SLC7A11/xCT at the crossroads of regulating redox homeostasis and nutrient dependency of cancer. Cancer Commun (Lond). 2018 38(1):12. doi: 10.1186/s40880-018-0288-x.

Koppula P, Zhuang L, Gan B. Cystine transporter SLC7A11/xCT in cancer: ferroptosis, nutrient dependency, and cancer therapy. Protein Cell. 2021 12(8):599-620. doi: 10.1007/s13238-020-00789-5.

Kose T, Vera-Aviles M, Sharp PA, Latunde-Dada GO. Curcumin and (-)- Epigallocatechin-3-Gallate Protect Murine MIN6 Pancreatic Beta-Cells Against Iron Toxicity and Erastin-Induced Ferroptosis. Pharmaceuticals (Basel). 2019 6;12(1):26. doi: 10.3390/ph12010026.

Kwon YS, Lee MG, Baek J, Kim NY, Jang H, Kim S. Acyl-CoA synthetase-4 mediates radioresistance of breast cancer cells by regulating FOXM1. Biochem Pharmacol. 2021 192:114718. doi: 10.1016/j.bcp.2021.114718.

Lang X, Green MD, Wang W, Yu J, Choi JE, Jiang L, Liao P, Zhou J, Zhang Q, Dow A, Saripalli AL, Kryczek I, Wei S, Szeliga W, Vatan L, Stone EM, Georgiou G, Cieslik M, Wahl DR, Morgan MA, Chinnaiyan AM, Lawrence TS, Zou W. Radiotherapy and Immunotherapy Promote Tumoral Lipid Oxidation and Ferroptosis via Synergistic Repression of SLC7A11. Cancer Discov. 2019 9(12):1673-1685. doi: 10.1158/2159-8290.CD-19-0338.

Lei G, Zhang Y, Koppula P, Liu X, Zhang J, Lin SH, Ajani JA, Xiao Q, Liao Z, Wang H, Gan B. The role of ferroptosis in ionizing radiation-induced cell death and tumor suppression. Cell Res. 2020 30(2):146-162. doi: 10.1038/s41422-019-0263-3.

Lei G, Mao C, Yan Y, Zhuang L, Gan B. Ferroptosis, radiotherapy, and combination therapeutic strategies. Protein Cell. 2021 12(11):836-857. doi: 10.1007/s13238-021-00841-y.

Lin W, Lu X, Yang H, Huang L, Huang W, Tang Y, Liu S, Wang H, Zhang Y. Metabolic heterogeneity protects metastatic mucosal melanomas cells from ferroptosis. Int J Mol Med. 2022 50(4):124. doi: 10.3892/ijmm.2022.5180.

Liu S, Zhang HL, Li J, Ye ZP, Du T, Li LC, Guo YQ, Yang D, Li ZL, Cao JH, Hu BX, Chen YH, Feng GK, Li ZM, Deng R, Huang JJ, Zhu XF. Tubastatin A potently inhibits GPX4 activity to potentiate cancer radiotherapy through boosting ferroptosis. Redox Biol. 2023 62:102677. doi: 10.1016/j.redox.2023.102677.

Nagane M, Kanai E, Shibata Y, Shimizu T, Yoshioka C, Maruo T, Yamashita T. Sulfasalazine, an inhibitor of the cystine-glutamate antiporter, reduces DNA damage repair and enhances radiosensitivity in murine B16F10 melanoma. PLoS One. 2018 13(4):e0195151. doi: 10.1371/journal.pone.0195151.

Qin S, He X, Lin H, Schulte BA, Zhao M, Tew KD, Wang GY. Nrf2 inhibition sensitizes breast cancer stem cells to ionizing radiation via suppressing DNA repair. Free Radic Biol Med. 2021 169:238-247. doi: 10.1016/j.freeradbiomed.2021.04.006.

Roh JL, Kim EH, Jang H, Shin D. Nrf2 inhibition reverses the resistance of cisplatin-resistant head and neck cancer cells to artesunate-induced ferroptosis. Redox Biol. 2017 11:254-262. doi: 10.1016/j.redox.2016.12.010.

Schäfer M, Dütsch S, auf dem Keller U, Navid F, Schwarz A, Johnson DA, Johnson JA, Werner S. Nrf2 establishes a glutathione-mediated gradient of UVB cytoprotection in the epidermis. Genes Dev. 2010 24(10):1045-58. doi: 10.1101/gad.568810.

Shimada K, Skouta R, Kaplan A, Yang WS, Hayano M, Dixon SJ, Brown LM, Valenzuela CA, Wolpaw AJ, Stockwell BR. Global survey of cell death mechanisms reveals metabolic regulation of ferroptosis. Nat Chem Biol. 2016 12(7):497-503. doi: 10.1038/nchembio.2079.

Singh B, Patwardhan RS, Jayakumar S, Sharma D, Sandur SK. Oxidative stress associated metabolic adaptations regulate radioresistance in human lung cancer cells. J Photochem Photobiol B. 2020 213:112080. doi: 10.1016/j.jphotobiol.2020.112080.

Spencer SL, Gaudet S, Albeck JG, Burke JM, Sorger PK. Non-genetic origins of cell-to-cell variability in TRAIL-induced apoptosis. Nature. 2009 459(7245):428-32. doi: 10.1038/nature08012.

Su J, Bian C, Zheng Z, Wang H, Meng L, Xin Y, Jiang X. Cooperation effects of radiation and ferroptosis on tumor suppression and radiation injury. Front Cell Dev Biol. 2022 10:951116. doi: 10.3389/fcell.2022.951116

Sui X, Zhang R, Liu S, Duan T, Zhai L, Zhang M, Han X, Xiang Y, Huang X, Lin H, Xie T. RSL3 Drives Ferroptosis Through GPX4 Inactivation and ROS Production in Colorectal Cancer. Front Pharmacol. 2018 9:1371. doi: 10.3389/fphar.2018.01371

Takahashi N, Cho P, Selfors LM, Kuiken HJ, Kaul R, Fujiwara T, Harris IS, Zhang T, Gygi SP, Brugge JS. 3D Culture Models with CRISPR Screens Reveal Hyperactive NRF2 as a Prerequisite for Spheroid Formation via Regulation of Proliferation and Ferroptosis. Mol Cell. 2020 80(5):828-844.e6. doi: 10.1016/j.molcel.2020.10.010.

Tang D, Chen X, Kang R, Kroemer G. Ferroptosis: molecular mechanisms and health implications. Cell Res. 2021 31(2):107-125. doi: 10.1038/s41422-020-00441-1.

Wang H, Jiang H, Van De Gucht M, De Ridder M. Hypoxic Radioresistance: Can ROS Be the Key to Overcome It? Cancers (Basel). 2019 11(1):112. doi: 10.3390/cancers11010112.

Wang L, Liu Y, Du T, Yang H, Lei L, Guo M, Ding HF, Zhang J, Wang H, Chen X, Yan C. ATF3 promotes erastin-induced ferroptosis by suppressing system Xc. Cell Death Differ. 2020 27(2):662-675. doi: 10.1038/s41418-019-0380-z.

Wu Y, Yu C, Luo M, Cen C, Qiu J, Zhang S, Hu K. Ferroptosis in Cancer Treatment: Another Way to Rome. Front Oncol. 2020 10:571127. doi: 10.3389/fonc.2020.571127.

Xie L, Song X, Yu J, Guo W, Wei L, Liu Y, Wang X. Solute carrier protein family may involve in radiation-induced radioresistance of non-small cell lung cancer. J Cancer Res Clin Oncol. 2011 137(12):1739-47. doi: 10.1007/s00432-011-1050-9.

Yang WS, Stockwell BR. Synthetic lethal screening identifies compounds activating iron-dependent, nonapoptotic cell death in oncogenic-RAS-harboring cancer cells. Chem Biol. 2008 15(3):234-45. doi: 10.1016/j.chembiol.2008.02.010.

Yang WS, SriRamaratnam R, Welsch ME, Shimada K, Skouta R, Viswanathan VS, Cheah JH, Clemons PA, Shamji AF, Clish CB, Brown LM, Girotti AW, Cornish VW, Schreiber SL, Stockwell BR. Regulation of ferroptotic cancer cell death by GPX4. Cell. 2014 156(1-2):317-331. doi: 10.1016/j.cell.2013.12.010.

Yang F, Xiao Y, Ding JH, Jin X, Ma D, Li DQ, Shi JX, Huang W, Wang YP, Jiang YZ, Shao ZM. Ferroptosis heterogeneity in triple-negative breast cancer reveals an innovative immunotherapy combination strategy. Cell Metab. 2023 3;35(1):84-100.e8. doi: 10.1016/j.cmet.2022.09.021.

Ye LF, Chaudhary KR, Zandkarimi F, Harken AD, Kinslow CJ, Upadhyayula PS, Dovas A, Higgins DM, Tan H, Zhang Y, Buonanno M, Wang TJC, Hei TK, Bruce JN, Canoll PD, Cheng SK, Stockwell BR. Radiation-Induced Lipid Peroxidation Triggers Ferroptosis and Synergizes with Ferroptosis Inducers. ACS Chem Biol. 2020 15(2):469-484. doi: 10.1021/acschembio.9b00939

Zhang Y, Shi J, Liu X, Feng L, Gong Z, Koppula P, Sirohi K, Li X, Wei Y, Lee H, Zhuang L, Chen G, Xiao ZD, Hung MC, Chen J, Huang P, Li W, Gan B. BAP1 links metabolic regulation of ferroptosis to tumour suppression. Nat Cell Biol. 2018 20(10):1181-1192. doi: 10.1038/s41556-018-0178-0.

Zilka O, Shah R, Li B, Friedmann Angeli JP, Griesser M, Conrad M, Pratt DA. On the Mechanism of Cytoprotection by Ferrostatin-1 and Liproxstatin-1 and the Role of Lipid Peroxidation in Ferroptotic Cell Death. ACS Cent Sci. 2017 3(3):232-243. doi: 10.1021/acscentsci.7b00028.

Zou Y, Palte MJ, Deik AA, Li H, Eaton JK, Wang W, Tseng YY, Deasy R, Kost-Alimova M, Dančík V, Leshchiner ES, Viswanathan VS, Signoretti S, Choueiri TK, Boehm JS, Wagner BK, Doench JG, Clish CB, Clemons PA, Schreiber SL. A GPX4-dependent cancer cell state underlies the clear-cell morphology and confers sensitivity to ferroptosis. Nat Commun. 2019 10(1):1617. doi: 10.1038/s41467-019-09277-9.